Available online at www.sciencedirect.com

ScienceDirect

journal homepage: www.elsevier.com/locate/he

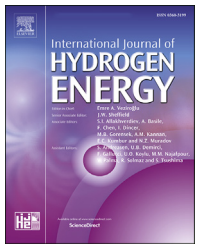

Review Article

Prospects of enhancing the understanding of material-hydrogen interaction by novel in-situ and in-operando methods

Agustina Massone [a,b,*], *Daniel Kiener* [b]

[a] *Materials Center Leoben, Forschungs GmbH, Roseggerstrasse 12, 8700, Leoben, Austria*
[b] *Department Materials Science, Chair of Materials Physics, Montanuniversität Leoben, Jahnstrasse 12, 8700, Leoben, Austria*

HIGHLIGHTS

- In-situ and in-operando methods were reviewed for studying material-H interaction.
- Fundamental models of the H charging mechanisms are discussed.
- Potential benefits for small scale testing for energy related material development.

ARTICLE INFO

Article history:
Received 29 July 2021
Received in revised form
15 November 2021
Accepted 11 January 2022
Available online 5 February 2022

Keywords:
Hydrogen
Energy sources
In-situ and in-operando methods
Electrochemical charging
Plasma charging

ABSTRACT

A main scientific and technical challenge facing the implementation of new and sustainable energy sources is the development and improvement of materials and components. In order to provide commercial viability of these applications, an intensive research in material-hydrogen (H) interaction is required. This work provides an overview of recently developed in-situ and in-operando H-charging methods and their applicability to investigate mechanical properties, H-absorption characteristics and H embrittlement (HE) susceptibility of a wide range of materials employed in H-related technologies, such as subsea oil and gas applications, nuclear fusion and fuel cells.

* *Corresponding author*. Materials Center Leoben, Forschungs GmbH, Roseggerstrasse 12, 8700, Leoben, Austria.
E-mail addresses: massoneagustina@gmail.com, agustina.massone@stud.unileoben.ac.at (A. Massone).

https://doi.org/10.1016/j.ijhydene.2022.01.089

Contents

Introduction 10098
Current status of in-situ and in-operando methods for studying H effect on materials 10099
H absorption mechanisms 10102
Applicability of novel in-situ methods towards challenges in H-related energy sources 10106
Subsea oil and gas 10106
Nuclear power 10106
Fuel cell technology 10106
Storage 10106
Automotive industry 10107
Conclusions 10107
Declaration of competing interest 10108
Acknowledgments 10108
References 10108

Introduction

The increasing demand for energy supply leads to the necessity of providing more sustainable energy sources [1]. The main energy sources used nowadays include coal, oil, natural gas and nuclear energy [2]. These energy sources are largely responsible for global warming as carbon dioxide (CO_2) is emitted from these fossil fuels. To reduce greenhouse emissions, it is necessary to find an alternative to the present fossil fuel technologies, and many political and technological measures have been adopted throughout the world to decrease the amount of CO_2.

H is expected to play a key role as a potential future energy source [3–7]. It can be generated from renewable sources and produces electricity when reacting with oxygen in fuel cells, being water the only by-product [8]. H based electrical energy has many advantages over other energy sources: Higher efficiency compared to diesel (45%) or gasoline (22%), higher specific energy content than gasoline and diesel and, as mentioned above, it produces only renewable waste [9].

With the introduction of H as an energy source, H technology plays an important role in many applications, and the interaction between H and the materials used in such applications needs to be considered and investigated to ensure a successful technology implementation. For instance, in comparison with other fuels, H is difficult to store and transport. In this scenario, H storage is considered as one of the most crucial and technically challenging barriers to the widespread use of H as an effective energy carrier [10,11]. As such, a future H economy will require two types of storage systems: one for transportation and one for stationary applications.

For transportation applications, the material should be capable of containing a high weight percent and a high-volume density of H, and also be able to rapidly absorb and desorb it at room environment conditions. Ideally, such material should be created using low energy-preparation methods, have a good thermal conductivity, be safe and reusable on exposure to air, and have the ability to be recycled and reused [8].

There are several different established storage methods [12], which can be categorized either as physical storage (compressed gas and cryogenic storage) or as storage in solid materials (physisorption and chemical storage). Materials used in physical storage applications are mainly selected for their mechanical properties in order to improve the structure of the vessels. While chemical storage materials are selected primarily for their physical properties [13].

Nuclear energy is another potential alternative for electric power generation. Compared to energy produced by combustion, nuclear fission can produce about ten million times more energy [14]. In addition to high specific energy, nuclear energy has the advantage of not releasing CO_2 into the atmosphere. Another advantage is that the fuel can be reprocessed and reused, conserving natural resources. The downside of this technology is the long-term storage of nuclear waste [14]. The selection of candidate materials for advanced nuclear reactors requires a thorough understanding of their performance under severe environmental conditions combined with radiation damage [15].

Oil and gas production also play a key role in the growing energy demand. Even though this source is not renewable, this industry sector is still popular and important reserves of oil and gas are left to be discovered and exploited. With the depletion of the continental shelf reserves, offshore exploration and production is moving to ultra deepwater. These are usually challenging locations and under extreme environments, facing high pressure and/or high temperature [16–18], and require the development of new materials, methodologies and technologies.

As can be anticipated from the requirements mentioned above, in conjunction with the tendency of H to cause material embrittlement, the main scientific and technical challenges facing the described potential energy sources are cost reduction and increased durability of materials and components. This requires intense research regarding the development of

improved or new materials, to provide commercial viability of these applications.

Small-scale testing of materials has gained prominence, initially by providing a methodology to examine small material volumes [19–23]. This was widely explored and opened new possibilities to study mechanical properties and deformation mechanisms of materials. For example, Korte et al. [24] performed micropillar compression to examine the plastic flow of individual phases. Studying plasticity in brittle materials requires the suppression of cracking. By making micropillars with diameters in the order of a micron, not only cracking is suppressed, but also it is possible to produce single crystal test samples [25,26]. With this testing method, they were able to study the differences in flow behavior in different hard phases. Furthermore, ion beam radiation damage has been investigated [27] by combining nano-compression with in-situ observation of the deformation behavior. Due to the limited penetration depth of ions, testing small volumes is essential to assess the properties of ion beam irradiated materials. Micropillar compression can also be used to study individual phases. For instance, Jun et al. [28] investigated the local strain rate sensitivity of the α phase in a dual-phase Ti alloy. Since deformation of Ti alloys is elastically and plastically rather anisotropic at the grain scale [29], the strain rate sensitivity could differ with grain orientation and slip systems, making the local investigation using small-scale testing crucial. Micropillar compression has also been used to analyse different deformation mechanisms by designing micropillars with specific orientation and microstructure [30], allowing examination of variable deformation mechanisms in non-trivial crystal structures.

To study nanostructured materials, such as thin films, small-scale testing methods are designated as best suited approaches to provide valuable insights into the mechanical behavior. Glechner et al. [31] investigated the mechanical properties of transition-metal carbide and nitrides using various micromechanical testing methods. They carried out nanoindentation, uniaxial compression tests on nano-pillars and bending tests on nano-cantilever beams. In this way, they were able to compare the mechanical behavior of different thin films. Furthermore, small-scale testing can be used for local property mapping, for example using nanoindentation. This technique can be a very useful in the study of the effects of H on deformation since it is very localized and can be used to test small volumes. Maier-Kiener et al. [32] performed nanoindentation testing to analyse the phase stability of a nanocrystalline high-entropy alloy by detecting phase decomposition via changes in hardness, Young's modulus and strain rate sensitivity. Spherical nanoindentation can also be used to examine local flow properties by converting hardness to representative stress in materials with small internal-length scales [33]. Local processes and details happening during crack propagation can also be studied with micromechanical testing. For example, recently Burtscher et al. [34] tested miniaturized notched cantilevers to investigate the effect of different interface types on crack propagation.

It can be anticipated that small-scale testing offers a wide number of possibilities to study deformation mechanisms. The present work will give an overview of the suitability and potential implementation of different recently developed small-scale in-situ and in-operando H-charging methods to study the interaction of H with a wide range of materials that are currently used in H-related applications, such as structural and gas applications, H storage, in the automotive industry, among others. Fig. 1 depicts a scheme of the applicability of the methods in the mentioned applications. Notably, due to their versatile nature, they can be used to study the mechanical properties, H absorption characteristics and HE susceptibility of almost any material.

Current status of in-situ and in-operando methods for studying H effect on materials

To study the interaction between H and any material, environmental, mechanical, and material aspects should be well defined [35] in order to ensure a conclusive analysis. One of the first in-situ studies controlling these three factors was performed by Vehoff et al. [36]. They developed a bulk method for studying crack propagation under a controlled environment and controlled plastic strain conditions. Nevertheless, it was only defined for macroscopic single crystals with specific orientation and challenging to apply on complex microstructures. Robertson, Birnbaum and Sofronis [37,38] also developed an in-situ approach for small scale investigations using straining experiments in an environmental transmission electron microscope (TEM). With this technique it was possible to directly observe the effect of H on dislocations, which seems to play an important role in HE of metals [35]. However, there were some uncertainties in the experimental conditions of their approach. For instance, the interpretation of crack growth was difficult, as the electron beam dissociated the H molecules, making the environmental conditions not defined well enough, and although the observation was with high-resolution, the field of view was limited to the transparent region of the sample, which is typically in the μm regime.

Following the in-situ approaches, another in-operando micro- and nanoscale mechanical testing method widely used in studying HE is the combination of electrochemical charging with nanoindentation testing [35,39–44], as shown in Fig. 2a. Nanoindentation is capable of resolving dislocation nucleation in samples with low dislocation density. Furthermore, this technique offers noticeable advantages such as the possibility to perform multiple tests within a single grain. And even though the volume of deformation is small, it is large enough to activate multiple slip systems under the indenter [39]. The primary focus of most of these studies was on the effect of H on the pop-in load in the load-displacement curves, which corresponds to the homogeneous dislocation nucleation at the onset of plasticity. These dislocations are nucleated from dislocation-free material. However, this analysis only applies for coarse-grained materials with a low dislocation density.

With nanoindentation it is also possible to investigate the effect of H on the hardness and Young's modulus of the materials. The evaluation of the effect of H on hardness can be correlated to the effect of H on dislocation mobility as well as solid solution strengthening or softening. Ebner et al. [40]

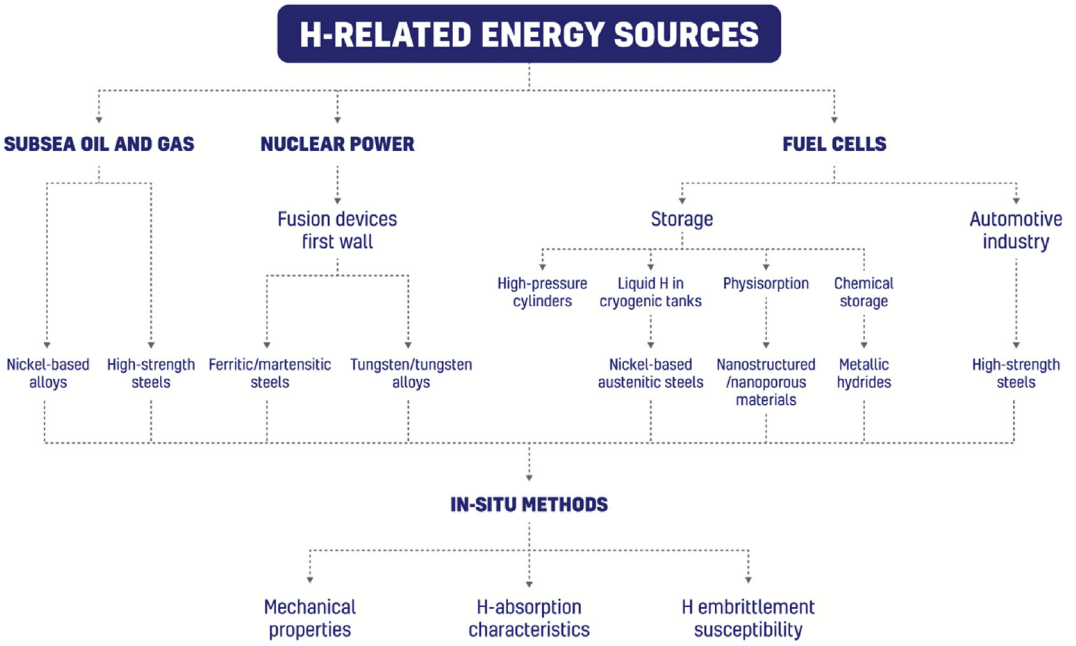

Fig. 1 – Applicability of in-situ methods to materials used in H-related applications.

developed an in-situ and in-operando method, Fig. 2b, to perform electrochemical nanoindentation tests with continuous stiffness measurement, which allows a continuous measurement of Young's modulus and hardness over indentation depth. With such measurement, additional information on external influences, such as frame stiffness or depth-dependent properties in more complex material systems can be obtained. Combining electrochemical charging and nanoindentation strain rate jump tests on a nickel-based alloy, Ebner et al. [45] proved that hardness and strain-rate sensitivity increased in the presence of H, concluding that the deformation mechanism was affected, and that H led to a more localized deformation.

Another in-situ and in-operando method based on nanoindentation was developed by Duarte et al. [46]. They built an electrochemical setup similar to the one in Fig. 2a, which they referred to as "front-side" charging, and also designed a new one based on a "back-side" charging approach. In this approach, the electrolytic cell was placed below the sample and H reaches the upper testing surface through diffusion. The main advantage of this charging method is that the testing surface is not affected by the charging process, which is one of the major drawbacks of electrochemical charging. To compare both charging types, they tested a bcc FeCr alloy with both setups. Even though they noticed a similar trend in the pop-in analysis, an increase in hardness and negligible change in Young's modulus was obtained with the back-side charging, while a decrease in hardness and Young's modulus was achieved when using the front-side charging. The results obtained with the latter were attributed to surface evolution or material damage during H charging. The main disadvantage of the back-side charging, compared with the front-side version, is the long charging time required for H diffusion in alloys with low H diffusivity.

Even though these approaches combine in-situ H charging and mechanical testing, it is not possible to have high-resolution observation during the tests to investigate the effect of H on the microstructure. To overcome this limitation, Kim et al. [47] developed an in-situ and in-operando technique to perform both microstructural and mechanical analysis during electrochemical H permeation, as depicted in Fig. 2c. During electrochemical charging, liquid electrolytes can contaminate sample surfaces by corrosion. Therefore, they charge the samples from the bottom surface to provide an objective surface without contamination for high-resolution observation. They used their technique to perform H mapping, investigate H-induced phase transformation, and conducted in-situ and in-operando nanoindentation experiments within a scanning electron microscope (SEM).

H distribution plays an important role in HE susceptibility. For instance, in materials with more than one phase, such as duplex stainless steels consisting of ferrite and austenite, the H diffusivity differs largely in both phases. Knowledge of the H distribution and the preferred diffusion paths, for example employing silver decoration [48,49] with the method developed by Kim et al. can help to detect the weak phases or features in the microstructure. Furthermore, real-time SEM imaging during H charging can provide the observation of phase transformations, while electron backscatter diffraction (EBSD) analysis can document the formation of hydrides in hydride forming materials. Moreover, with in-situ H charging and in-situ nanoindentation in an SEM, the effect of H on mechanical properties at a specific microstructural feature of interest can be investigated.

Deng et al. [50,51] performed in-situ and in-operando microcantilever bending tests with nanoindentation in an environmental SEM (ESEM) to have a full observation of potential H effects on the deformation process and microstructure evolution

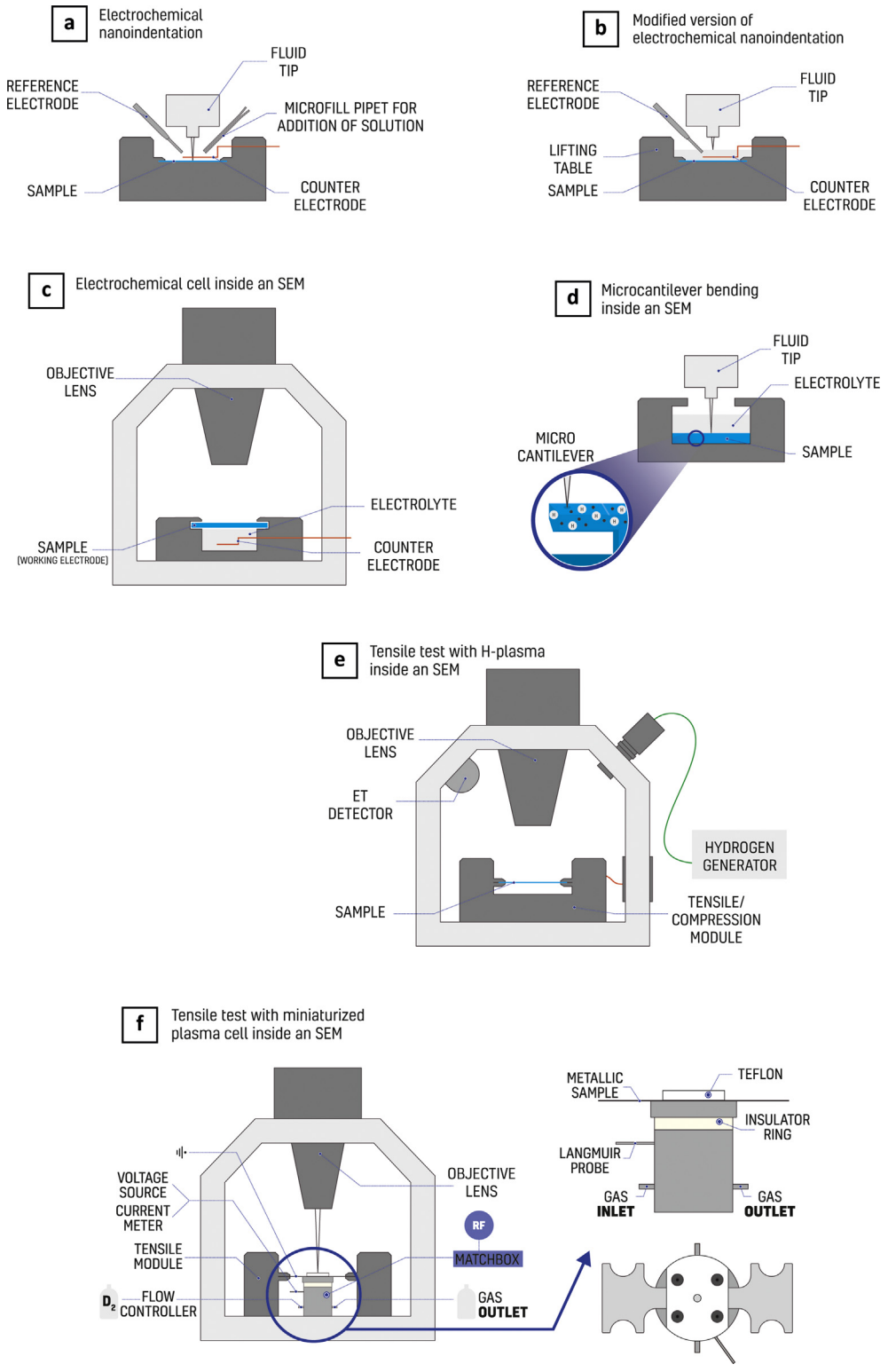

Fig. 2 – Schemes on in-situ and in-operando H methods. (a) Nanoindentation combined with electrochemical charging. (b) Modified version of electrochemical nanoindentation test. (c) Electrochemical cell inside an SEM. (d) Microcantilever bending test inside an ESEM. (e) Tensile test combined with H-plasma inside an ESEM. (f) Tensile test with a miniaturized plasma cell inside an SEM.

on a FeAl alloy, Fig. 2d. Atomic H was produced by the reaction of Al with water vapor, which was used as the default environment in the ESEM. Micro-cantilever bending tests with in-situ H charging provide a good compromise by using micro-sized samples, small enough to capture H effects, while at the same time having enough volume capacity to avoid the disadvantages from ETEM tests, which do not ensure a certain constant strain/stress state and can have proximity effects since smaller samples are used. The downside of their method is that it is only applicable to materials that produce atomic H by reaction with water vapor. Hajilou et al. [52] also performed micro-cantilever bending tests, in this case with an in-situ miniaturized electrochemical charging cell, to investigate the effect of H on the crack propagation of notched micro-cantilevers. To maintain the dimensional integrity avoiding local corrosion on the sample, they used a glycerol electrolyte instead of aqueous solutions. With their approach, they were able to confine the H interaction with the sample to a localized region in the vicinity of the notch and allow observation of the H effect with high resolution.

Another strategy of in-situ testing to allow high-resolution observation during mechanical testing is with H-plasma charging [53–56]. Wan et al. [53] developed an in-situ and in-operando method using low pressure H-plasma in an ESEM chamber to allow in-situ mechanical testing with in-situ H charging. They connected a plasma cleaner to the SEM chamber, and a H generator was connected to the working gas inlet of the plasma cleaner, as shown in Fig. 2e. A tensile specimen was then installed into a tensile/compression module. The limitation in their method is to have an in-situ observation by using normal SEM mode. Due to high flammability of H, they had to evacuate the chamber before imaging. Therefore, rather than in-situ imaging, it was limited to in-situ in position and ex-situ in environment. An important advantage of their charging method is that, since the plasma phase is not directly injected on the specimen surface, the surface would have the least possible damage from exposure to plasma and only the active particles could take part in the reaction. With their method, they were able to perform tensile tests as well as fatigue crack growth experiments.

Massone et al. [55] also performed in-situ and in-operando studies using plasma charging. Their method, depicted in Fig. 2f, also consists of in-situ mechanical testing and in-situ H charging in the SEM. An in-situ observation using the SEM is in this case possible while charging. They built a miniaturized plasma cell in which a plasma is ignited through a radio frequency discharge. The tensile sample, acting as the grounded electrode of the setup, is charged from the bottom, leaving a contamination-free top surface for SEM observation, similar to the unidirectional charging approaches in Refs. [46,47]. A disadvantage of these concepts, where the samples are charged in a unidirectional way, is that a H concentration gradient is created, with the objective surface having the lowest concentration. Nonetheless, a constant supply of H leads to a dynamic equilibrium of the H concentration, thereby the charging time to detect H effects on the objective surface depends on the thickness of the sample and the H diffusivity. A difference between the methods from Refs. [47,55] is that in the first case, the sample can be tested until fracture, since the plasma turns off automatically when the sealing of the plasma cell is lost. In the second case, on the other hand, only non-destructive mechanical tests can be conducted since the sample isolates the electrolyte from the vacuum environment.

Fig. 3 depicts selected examples obtained with some of the methods described above. For example, Fig. 3a shows H partitioning results from the method from Ref. [47] (electrochemical cell inside an SEM). The microstructure of a duplex stainless steel before H charging is shown in Fig. 3a1, while Fig. 3a2 corresponds to an image after H charging using the silver decoration technique. Thereby, H atoms react with silver ions that were previously deposited on the surface of the H-charged sample. The silver nanoparticles formed in the reaction can be observed as white dots in the microstructure. As shown in Fig. 3a2, these silver nanoparticles are formed on the ferritic phase and preferentially along phase boundaries. Thus, with this method the distribution of H and preferential diffusion paths can be easily mapped.

Fig. 3b shows results of micro-cantilever bending tests from Ref. [52], with Fig. 3b1 tested under air and Fig. 3b2 tested with H charging. From the post mortem analysis it is evident that H affected the ductility of the sample, being a Fe-3 wt% Si alloy. In fact, the amount of emitted dislocations (correlating with the misorientation mappings) from the notch tip was less than for the test under air and more localized (compare last row images).

H absorption mechanisms

In the study of H-material interactions, the H source is a key parameter to control. Knowledge of maximum H concentrations and H concentration profiles achieved by different charging methods for the setups described in the previous section is crucial in the analysis of the results. For instance, the understanding of H concentration profiles can give a hint on the failure initiation points within a sample. Moreover, knowledge of the maximum H concentration can be insightful as an indication of the degree of embrittlement or the critical amount of H that can be absorbed by a certain material. Therefore, it is instructive to understand the different involved supply methods and their limits.

The sources of H in the previously described methods are either via electrochemical charging or through a H plasma. In electrochemical charging, a H evolution reaction may proceed through the following reaction steps in a neutral/alkaline solution [57]:

$$H_2O + M + e^- \leftrightarrow MH_{ads} + OH^+ \quad \text{Volmer} \tag{1}$$

$$MH_{ads} + H_2O + e^- \leftrightarrow H_2 + OH^- + M \quad \text{Heyrovsky} \tag{2}$$

Equation (1) corresponds to H adsorption, which is followed by electrochemical desorption reactions, equation (2). The last step of the process is the absorption of H from the surface to the bulk. Fig. 4 shows a scheme of the H evolution reaction in these two steps during electrochemical charging in a neutral/alkaline solution. By controlling the electrolyte solution concentration, the potential and current density and the charging time, different H concentrations can be obtained.

In plasma charging, on the other side, ion-driven permeation (IDP) takes place. This differs from electrochemical H

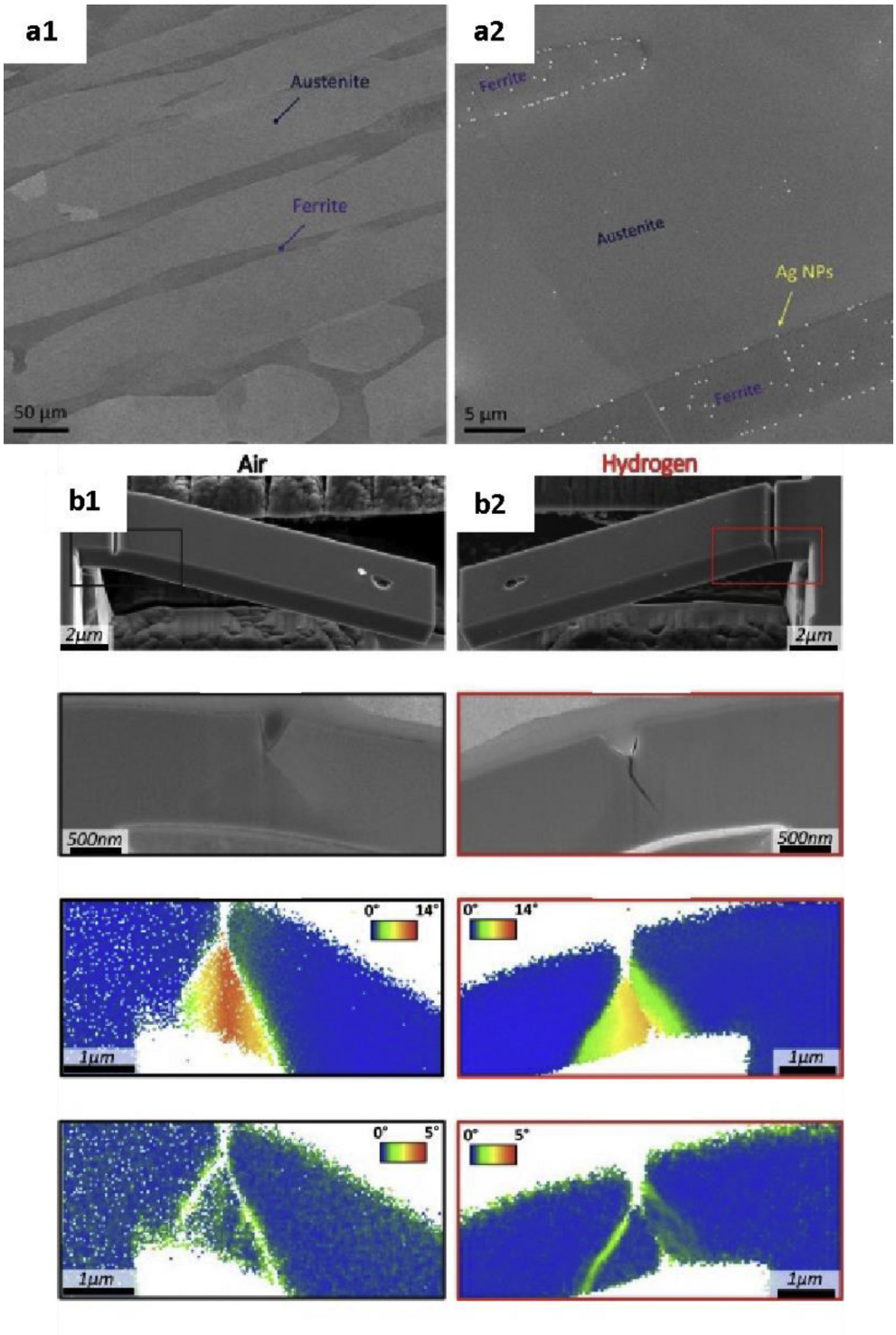

Fig. 3 – a. Example of results obtained for a duplex steel with electrochemical nanoindentation experiments within an SEM [47]. (a1) Back-scattered electron image before H charging. (b1) Secondary electron image after H charging highlighting H-induced silver nanoparticle decoration. b. Exemplary data gained using micro-cantilever bending tests on an Fe-3 wt% Si alloy [52]. (b1) SEM, reference orientation deviation and Kernel average misorientation images of a H free micro-cantilever. (b2) SEM, reference orientation deviation and Kernel average misorientation images of H charged micro-cantilever. Figures reprinted with permission.

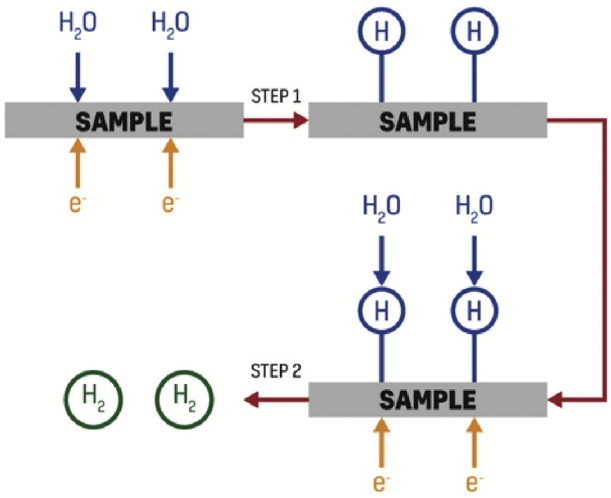

Fig. 4 – H evolution reaction in Volmer-Heyrovsky mechanism during electrochemical charging.

absorption and gas-driven permeation (GDP) in the way by which H isotopes enter the material. In GDP, the molecules of H_2 must be adsorbed on the surface, dissociate and be absorbed in the bulk, resulting in a comparatively small permeation rate. On the contrary, in IDP H ions enter the bulk with excess energy, resulting in a comparatively large permeation rate [58]. Depending on the relative rate of recombination (R) and diffusion (D) on both sides of the samples, one in contact with plasma and the other subjected to observation, the IDP process of H isotopes can be divided into three categories.

- RR regime: Rate limited by recombination on both sample sides.
- RD regime: Rate limited by recombination on the plasma-exposed side and diffusion on the observation side.
- DD regime: Rate limited by diffusion on both sides.

Usually, the maximum permeation flux appears in the RR regime and the minimum in the DD regime, respectively. The IDP transport regime of H isotopes depends on the incident ion flux and parameters of the plasma-exposed side (mean implantation depth, recombination coefficient and diffusion coefficient), as well as parameters of the other side (sample thickness, recombination coefficient and diffusion coefficient).

Fig. 5 shows schematically the H concentration profile for electrochemical charging (Fig. 5a) and the IDP model at steady-state (Fig. 5b) across the thickness of the material. In the IDP model, Φ_i is the incident ion flux, Φ_r is the reflected flux and Φ_p the permeated flux. In steady-state, the condition $\Phi_i = \Phi_r + \Phi_p$ is obeyed.

Equations (4) and (5) show the maximum concentration for RR/RD and DD regimes, respectively.

$$C_{RR/RD} = \sqrt{\frac{\varphi_i}{k_f}} \tag{4}$$

$$C_{DD} = \frac{r_{impl}\varphi_i}{D_f} \tag{5}$$

Hereby, φ_i is the incident flux, k_f a recombination coefficient, r_{impl} the mean implantation depth and D_f the diffusion coefficient. The equations for RR and RD regimes are the same since usually the recombination coefficient on the plasma-exposed side is much larger than on the observation side [58].

As shown in Fig. 5b, the maximum H concentration for IDP appears at a distance $x = r_{impl}$ (mean implantation depth), which can be calculated using for example a Monte-Carlo program [59]. The maximum concentration depends only on the incident ion flux and the parameters at the plasma-exposed side (r_{impl}, k_f and D). The parameters on the observation side do not affect the maximum concentration at steady-state. When considering the plasma charging method from Ref. [55], the other side of the plasma-charged surface in is under vacuum so the concentration on the top-observed surface is considered to be 0.

Baskes et al. [60] classified the metals as exothermic metals (e.g. Zr and Ti), which have no entry barrier for an H atom entering the bulk; or endothermic metals (e.g. Ni, Fe, Al), where the barrier is the sum of the solution and diffusion activation energies. For exothermic metals, surface recombination is the rate-limiting step and large bulk concentrations may be easily obtained. Contrarily, surface recombination is not the limiting step for the endothermic metals. Fig. 6 depicts the recombination constant and H concentration as a function of inverse temperature for various metals for an ion flux of 10^{16} $m^{-2}s^{-1}$ [60]. Notably, this is the same flux expected with the plasma cell from the method described in Ref. [55]. It is shown in Fig. 6 that exothermic metals, such as Zr and Ti, can

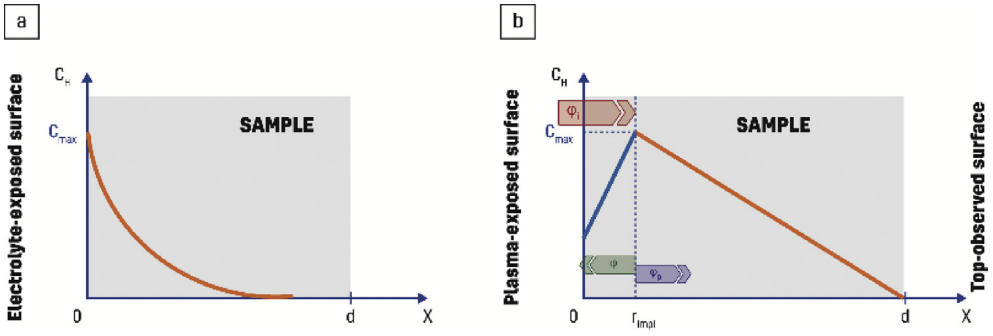

Fig. 5 – H concentration profile for (a) an electrochemical charged sample and (b) the model of ion-driven permeation at steady-state with plasma charging.

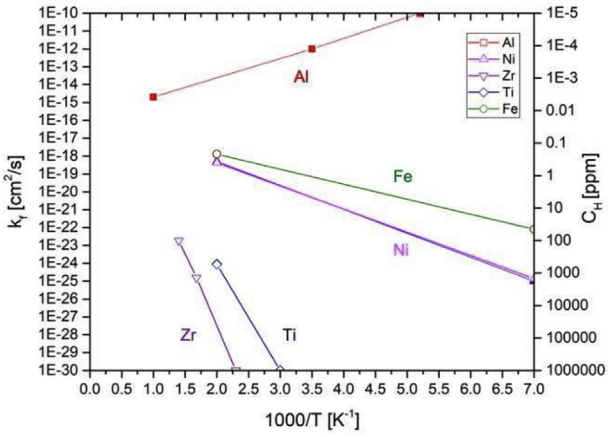

Fig. 6 – Recombination constant k_f as a function of inverse of temperature for various metals and H concentration for an ion flux of 10^{16} $m^{-2}s^{-1}$. This figure has been reproduced from Ref. [60] with the author's consent.

reach a much higher surface concentration than their endothermic counterparts.

This analytical model by Baskes [60] has been applied to the in-situ H plasma charging method from Ref. [55] and compared with simulation results [61], and it has been confirmed that the simulated concentration of lattice H shows a very good agreement with the analytical calculation. Nevertheless, it is important to mention that this model only considers the solute fraction concentration. When considering the total concentration, i.e., H stored in interstitial lattice positions and H in traps, the values tend to be higher. Therefore, the following calculations of H absorption will correspond to a lower bound of the expected total concentration, since any material with lattice defects can trap H. For instance, interfaces of non-metallic inclusions are strong trapping sites for H with high trap activation energy; while lattice imperfections, grain boundaries, dislocations and microvoids are shallow traps [62].

The respective recombination coefficient k_f for the concentrations corresponding to RR/RD regimes was calculated according to Ref. [63]:

$$k_f = 4.8 \times 10^{-21} exp(\frac{0.48\ (eV)}{kT}) \quad (6)$$

where k is the Boltzmann constant and T the temperature.

Table 1 shows the calculated H concentrations using equations (4)–(6) for different materials at room temperature, while Fig. 7 depicts the transport regimes as function of temperature for a list of materials for an ion flux of 10^{20} m^{-2} s^{-1}. The materials in Table 1 were classified by their transport regime according to Fig. 7. Nevertheless, both lattice concentrations from equations (4) and (5) are displayed. It can be seen that all H concentration values corresponding to the DD regime are larger than the other regimes. The transport parameters with the corresponding regime determination depend on the temperature and the ion flux [58]. Therefore, it is not possible to determine a specific transport regime for each material. For a general overview, at temperatures below ~100 °C, for example, W, Al, Mo and Ni, among others, exhibit a DD characteristic and therefore, a higher H concentration is expected in these materials in comparison with the other materials in Table 1.

Table 1 – Lattice H concentrations for RR/RD and DD permeation regimes.

	Material	$C_{lattice}$ RR/RD [wppm]	$C_{lattice}$ DD [wppm]
DD regime	*Al*	2.1E-04	11760.1
	Mo	5.6E-05	0.8
	Ni	6.4E-05	734.3
	W	3.0E-05	466.5
RD/RR regimes	*Fe*	7.3E-05	8.1E-04
	Mg	3.3E-04	2.6E-03
	Pd	4.8E-05	0.2
	Pt	2.7E-05	0.1
	Ti	1.3E-04	3.5
	V	9.4E-05	1.1E-02
	Zr	8.8E-05	67.4
	Zircaloy	8.8E-05	27.4

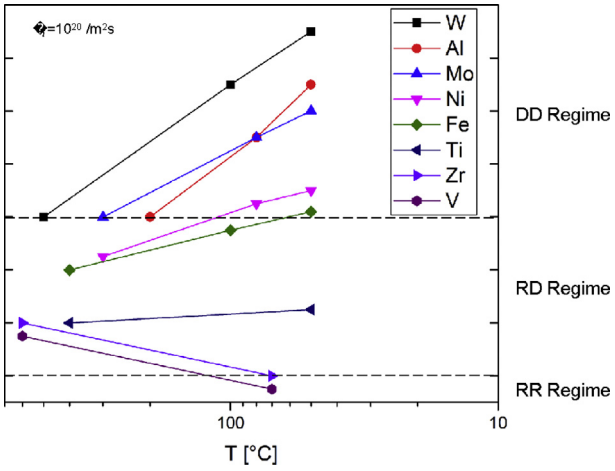

Fig. 7 – Transport regimes as a function of temperature for various materials [58,64]. This figure has been reproduced with the author's consent.

Asadipoor et al. [65] analysed the effect of H on a dual phase steel using ex-situ electrochemical charging, in-situ H-plasma charging and the combination of both. They demonstrated that with in-situ H-plasma charging, ductile fracture modes dominated over brittle modes, while with ex-situ electrochemical charging the brittle features were dominant. This indicated that plasma charging provides a lower H concentration than electrochemical charging. Nevertheless, as shown in Table 1, the upper limit of the range corresponding to the DD permeation regime is for most materials in the range of some wppm and thus high enough to produce an effect. This critical concentration to induce an observable H effect depends on the material, and not only on the strength level but also on the stress concentration factor [66].

Applicability of novel in-situ methods towards challenges in H-related energy sources

Subsea oil and gas

The first group of H-related energy sources shown in Fig. 1 corresponds to subsea oil and gas applications. Both nickel-based alloys and high-strength steels are among the most widely used materials in the oil and gas industry due to their outstanding mechanical properties and corrosion resistance. Deep wells that face corrosive environments, combined with high temperature and high pressure require high-strength materials with sufficient corrosion resistance that can withstand these harsh conditions [67]. Although Ni alloys fulfil these requirements, they are highly susceptible to HE [68–73]. Both solution annealed and aged conditions suffer a ductility loss in the presence of H, being the aged condition the most affected one. Even though the effect of H on Ni-based alloys has been widely studied [40,68–74], it is still an ongoing research and the implementation of the recently developed in-situ and in-operando methods could provide detailed information concerning the identification of the susceptible microstructural features and related modification to improve the alloys accordingly, thereby maximizing strength while avoiding detrimental H effects.

Nuclear power

Nuclear power has a very attractive potential to offer an environmentally friendly and safe energy source. A fusion power plant is free from concerns of exhaustion of fuels and production of CO_2. Furthermore, the product of the fusion reaction is helium, which is not radioactive, limiting the nuclear waste only to structural materials with neutron-induced activation [75]. Despite its advantages, there are still scientific and technological problems that must be solved before the successful commercialisation of fusion power. Among these, a challenge is the selection and development of the plasma facing materials, which will experience extreme heat and particle flux [76]. Plasma facing materials have two main roles, the protection of the first wall from high particle flux and the transportation of thermal energy away from the surface. Therefore, the selected materials should have high thermal conductivity and high resistance to erosion by particle bombardment [77].

Tungsten (W) is among the few possible plasma-facing candidate materials for the first wall of fusion devices [78]. It has very low solubility for H, high resistance to sputtering, high thermal conductivity and a high melting point. The amount of H that can be permanently retained in W is determined by the microstructure and the defect density in the material [79,80]. These defects act as trap sites for H, while excess solute H diffuses out even at room temperature. Radiation damage, either by incident H ions or by fast neutrons from the deuterium fusion reaction, can increase the natural defect density [78]. In this way, the number of trap sites for H retention is increased. The ions produce damage only in the near-surface regions due to saturation of the implantation zone leading to high stress fields, which produce cracks and gas-filled cavities [81]. These defects degrade the thermo-mechanical stability and also act as trap sites for H.

To study the suitability of W and W alloys as plasma-facing materials, the in-situ plasma charging methods from Refs. [53,55] can be used to simulate real (or close to real) conditions. In Ref. [55], deuterium plasma with different bias voltages can be ignited, giving the possibility to analyse the effect of different plasma parameters on the W-based materials. Also, the mechanical properties can be investigated, allowing the characterization of crack growth behavior and the mechanical stability after ion implantation. For instance, Yoon et al. [82] reported that W heavy alloys can suffer HE during the sintering process under H atmosphere. They showed that the elongation and UTS decreased in the presence of H, but the mechanical properties were restored by a heat treatment in vacuum. On the other hand, Li et al. [83] did not see any obvious HE effects on the W heavy alloy specimen after deuterium implantation under the analysed conditions. Nevertheless, they stated that the mechanism of deuterium transport and retention in tungsten heavy alloys is still not well understood, and the impact of deuterium implantation could vary under different experimental conditions. For this reason, the application of the in-situ plasma charging methods to investigate the embrittlement effect under different plasma conditions would provide valuable insights.

Fuel cell technology

Materials suitable for H storage must meet specific requirements in order to be used in the development of H-based technologies. In order to improve and maximize the efficiency of H storage systems, the characteristics and properties of the used materials, such as chemical composition, structure and morphology, and their thermodynamic and kinetic properties, have to be deeply understood [84]. In this context, the described in-situ and in-operando methods could provide valuable information regarding the mechanical properties, the microstructural characterization and H-absorption characteristics of potentially suitable materials.

Storage

Liquid H in cryogenic tanks. When considering the scheme from Fig. 1, the first group of materials for H storage suitable for implementing in-situ H charging methods are nickel-based austenitic steels. These are good candidates for the structural materials used in H storage systems based on liquid H, for components of fuel cell vehicles and stationary fuel cell systems and for equipment for H stations, H pipelines and transport systems [85,86]. In these systems, there is a direct exposure to high-pressure H and thus the austenitic stainless steels can suffer HE. Furthermore, austenitic stainless steels with low Ni content are generally metastable and form α'-martensite during deformation [87]. It has been reported that these steels are more susceptible to HE due to the faster H transport through the stress-induced martensite near the crack tip [85,86,88–93]. Even though the presented methods cannot exactly simulate the operating conditions under high-pressure H gas, as they use electrochemical or plasma charging, they can provide a detailed analysis of the microstructure evolution under deformation, a thorough examination of the H-material interaction

and related changes in the deformation and failure processes not easily accessible from post-mortem inspections.

Chemical storage. Metallic hydrides are the materials of choice used for chemical H storage [94–96]. When compared with liquid H storage, storage by absorption as chemical compounds has definite advantages from the safety perspective, since energy input is required to release H. Furthermore, metal hydrides have higher H-storage density than H gas or liquid H [97]. Liquid H requires an additional refrigeration unit to maintain a cryogenic state, adding weight and energy costs, resulting in a 40% energy loss [98].

Typical materials used in this application have the form MH, MH_2 and MH_3, with H fitting into octahedral or tetrahedral sites in the lattice or a combination of both, and also metallic hydrides of intermetallic compounds with the form AB_xH_n. The variation of elements allows tailoring the properties. Element A is usually a rare earth metal and tends to form a stable hydride. Element B is a transition metal and forms only unstable hydrides. This element plays a catalytic role in enhancing the hydriding/dehydriding characteristics, it can alter the equilibrium pressures for the H absorption/desorption, and it should enhance the stability of the alloys. Some examples of intermetallic compounds suited to form metallic hydrides are $LaNi_5$, ZrV_2, $ZrMn_2$, $TiMn_2$, $CeNi_3$, YFe_3, Y_2Ni_7, Th_2Fe_7, Y_6Fe_{23}, TiFe, ZrNi, Mg_2Ni, Ti_2Ni [84].

Hydride forming elements such as Ti, V and Zr are typically dominated by a RR or RD H transport regime at room temperature (Fig. 7). Therefore, a rather low H lattice concentration is expected with plasma charging in these materials, as shown in Table 1. The typical storage density of hydride materials is around 1.3–1.5% in weight of H [99], which is equivalent to 13,000–15000 wppm. This means that the gravimetric capacity of metal hydrides is much larger than the total amount of H that can be supplied by the previously mentioned methods. Nevertheless, they can provide the possibility to study characteristics of H-absorption and their relation with the materials microstructure, as the hydride formation will cause local modifications and potential damage in the material microstructure. Furthermore, assessment between different microstructural features in terms of H-absorption and hydride formation, as well as a comparison between different materials and alloys is possible and would benefit alloy selection microstructure design.

Automotive industry

The implementation of fuel cell technology in the automotive market is currently gaining worldwide popularity due to higher fuel efficiency, longer driving range and fast refuelling of fuel cell [100]. The next group of materials in the scheme in Fig. 1 represents high-strength steels. These are excellent candidates for the automotive industry, since they combine light weight and high strength, two essential characteristics in this industry. However, high strength steels are sensitive to HE and the higher the strength, the larger the susceptibility of the material. Their use is mainly limited by H, since it can reduce their ultimate tensile strength, ductility, fatigue strength and/or fracture toughness [101–104]. H uptake in autobody components can already result from assembling and/or finishing processes. Usually, advanced high strength steels are electroplated with a sacrificial metal, and H can be absorbed during this coating deposition. H can also be absorbed if the sacrificial coating corrodes during service and the exposed areas start acting as cathodic sites [105]. Moreover, during the painting process, cathodic reactions in water solution take place [106]. In this process, H is generated and part of it can be absorbed and diffused into the steel. Lovicu et al. [107] analysed the H concentration after a real production cycle (phosphatizing, electrodeposition and curing) in four types of advanced high-strength steels and showed that all samples absorbed less than 0.4 wppm. This value is lower than the usual critical concentrations, which are approximately between 1 and 4 wppm [107], suggesting a safe use to build body-in-white components. Nevertheless, the H uptake ability as well as the critical H concentrations to produce embrittlement are different for each steel.

Most of the studies made on high-strength steels are performed using ex-situ H charging [107–114] with the consequent risk of H outgassing taking place before testing the material, in particular in the case of steels with fast H-diffusion, such as ferritic grades. Therefore, this approach introduces an inherent error source that can alter the results.

Kim et al. [47] applied the electrochemical in-situ setup for a duplex stainless steel and a ferritic stainless steel. Even though they did not control the H concentration in the materials, they detected the presence of H at the objected surface of the duplex stainless steel using the silver decoration technique and saw an effect of H on the mechanical properties of the ferritic stainless steel. This proves that enough H can be absorbed even in fast diffusion steels via electrochemical charging to cause HE effects.

Considering the values of H lattice concentration with plasma charging in Table 1 for Fe, it can be seen that they are in the order of 10^{-5}-10^{-4} wppm. Nevertheless, as mentioned before, these correspond only to the lattice concentration, and the total value including traps is expected to be higher. For example, in Ref. [61] the total H concentration was calculated for a complex phase steel, resulting in 0.82 wppm, which was around a factor of 350 higher than the corresponding lattice H. This means that the plasma charging method from Ref. [55] provides a higher H concentration than the one expected in the painting process, opening the possibility to study H effect on steels in a condition similar to a real production cycle.

Conclusions

The current status of in-situ and in-operando H-charging methods has been reviewed, demonstrating their applicability to study the interaction of H with different materials used in a wide range of industrial applications. With the necessity of establishing new renewable energy sources based on H, it is essential to understand its effect on materials that must perform under H atmospheres. The described methods are based on electrochemical or plasma charging combined with mechanical testing, and in some cases even allow for in-situ observation and in-operando probing. Each of them has their own limitations and advantages, but all of them can provide previously inaccessible novel information of the effect of H on metallic materials. As such, they should be considered as valuable tools in our road towards a green energy society.

Declaration of competing interest

The authors declare that they have no known competing financial interests or personal relationships that could have appeared to influence the work reported in this paper.

Acknowledgments

The authors gratefully acknowledge the financial support under the scope of the COMET program within the K2 Center "Integrated Computational Material, Process and Product Engineering (IC-MPPE)" (Project No 859480). This program is supported by the Austrian Federal Ministries for Climate Action, Environment, Energy, Mobility, Innovation and Technology (BMK) and for Digital and Economic Affairs (BMDW), represented by the Austrian research funding association (FFG), and the federal states of Styria, Upper Austria and Tyrol. DK acknowledges funding by the European Research Council under the European Union's Horizon 2020 research and innovation program, grant agreement No. 771146 (TOUGHIT).

REFERENCES

[1] Dincer I. Renewable energy and sustainable development: a crucial review. Renew Sustain energy Rev 2000;4(2):157–75. https://doi.org/10.1016/S1364-0321(99)00011-8.
[2] Kaur M, Pal K. Review on hydrogen storage materials and methods from an electrochemical viewpoint. J Energy Storage 2019;23(March):234–49. https://doi.org/10.1016/j.est.2019.03.020.
[3] Momirlan M, Veziroglu TN. The properties of hydrogen as fuel tomorrow in sustainable energy system for a cleaner planet. Int J Hydrogen Energy 2005;30(7):795–802. https://doi.org/10.1016/j.ijhydene.2004.10.011.
[4] Winter CJ. Into the hydrogen energy economy - Milestones. Int J Hydrogen Energy 2005;30(7):681–5. https://doi.org/10.1016/j.ijhydene.2004.12.011.
[5] Rosen MA. The prospects for renewable energy through hydrogen energy systems. J Power Energy Eng 2015;3(4):373–7. https://doi.org/10.4236/jpee.2015.34050.
[6] Ball M, Wietschel M. The future of hydrogen - opportunities and challenges. Int J Hydrogen Energy 2009;34(2):615–27. https://doi.org/10.1016/j.ijhydene.2008.11.014.
[7] Midilli A, Dincer I. Key strategies of hydrogen energy systems for sustainability. Int J Hydrogen Energy 2007;32(5):511–24. https://doi.org/10.1016/j.ijhydene.2006.06.050.
[8] Edwards PP, Kuznetsov VL, David WIF. Hydrogen energy. Philos Trans R Soc A Math Phys Eng Sci 2007;365(1853):1043–56. https://doi.org/10.1098/rsta.2006.1965.
[9] Khalid F, Dincer I, Rosen MA. Analysis and assessment of an integrated hydrogen energy system. Int J Hydrogen Energy 2016;41(19):7960–7. https://doi.org/10.1016/j.ijhydene.2015.12.221.
[10] Crabtree GW, Dresselhaus MS, Buchanan MV. The hydrogen economy. Phys Today 2004;57(12):39–44. https://doi.org/10.1063/1.1878333.
[11] Zhang F, Zhao P, Niu M, Maddy J. The survey of key technologies in hydrogen energy storage. Int J Hydrogen Energy 2016;41(33):14535–52. https://doi.org/10.1016/j.ijhydene.2016.05.293.
[12] Züttel A. Materials for hydrogen storage. Mater Today 2003;6(9):24–33. https://doi.org/10.1016/S1369-7021(03)00922-2.
[13] Millet P. Hydrogen storage in hydride-forming materials. Woodhead Publishing Limited; 2014.
[14] Ben Anthony EJ. Handbook of climate change mitigation, vol. 4; 2016.
[15] Odette GR, Zinkle SJ. Structural alloys for nuclear energy applications. Elsevier; 2019.
[16] Bell JM, Chin YD, Hanrahan S. State-of-the-art of ultra deepwater production technologies. In: Proc. Annu. Offshore Technol. Conf. 2005-May; 2005. p. 1875–87. https://doi.org/10.4043/17615-ms.
[17] Iannuzzi M, Barnoush A, Johnsen R. Materials and corrosion trends in offshore and subsea oil and gas production. NPJ Mater Degrad 2017;1(1). https://doi.org/10.1038/s41529-017-0003-4.
[18] Perez TE. Corrosion in the oil and gas industry: an increasing challenge for materials. JOM (J Occup Med) 2013;65(8):1033–42. https://doi.org/10.1007/s11837-013-0675-3.
[19] Uchic MD, Dimiduk DM, Florando JN, Nix WD. Sample dimensions influence strength and crystal plasticity. Science 2004;305(5686):986–9. https://doi.org/10.1126/science.1098993.
[20] Dehm G, Jaya BN, Raghavan R, Kirchlechner C. Overview on micro- and nanomechanical testing: new insights in interface plasticity and fracture at small length scales. Acta Mater 2018;142:248–82. https://doi.org/10.1016/j.actamat.2017.06.019.
[21] Kiener D, Jeong J, Alfreider M, Konetschnik R, Oh SH. Prospects of using small scale testing to examine different deformation mechanisms in nanoscale single crystals—a case study in MG. Crystals 2021;11(1):1–15. https://doi.org/10.3390/cryst11010061.
[22] Uchic MD, Shade PA, Dimiduk DM. Plasticity of micrometer-scale single crystals in compression. Annu Rev Mater Res 2009;39:361–86. https://doi.org/10.1146/annurev-matsci-082908-145422.
[23] Greer JR, De Hosson JTM. Plasticity in small-sized metallic systems: intrinsic versus extrinsic size effect. Prog Mater Sci 2011;56(6):654–724. https://doi.org/10.1016/j.pmatsci.2011.01.005.
[24] Korte S, Clegg WJ. Studying plasticity in hard and soft Nb-Co intermetallics. Adv Eng Mater 2012;14(11):991–7. https://doi.org/10.1002/adem.201200175.
[25] Östlund F, et al. Ductile-brittle transition in micropillar compression of GaAs at room temperature. Philos Mag 2011;91(7–9):1190–9. https://doi.org/10.1080/14786435.2010.509286.
[26] Korte S, Barnard JS, Stearn RJ, Clegg WJ. Deformation of silicon - insights from microcompression testing at 25-500 °c. Int J Plast 2011;27(11):1853–66. https://doi.org/10.1016/j.ijplas.2011.05.009.
[27] Kiener D, Hosemann P, Maloy SA, Minor AM. In situ nanocompression testing of irradiated copper. Nat Mater 2011;10(8):608–13. https://doi.org/10.1038/nmat3055.
[28] Jun TS, Zhang Z, Sernicola G, Dunne FPE, Britton TB. Local strain rate sensitivity of single α phase within a dual-phase Ti alloy. Acta Mater 2016;107:298–309. https://doi.org/10.1016/j.actamat.2016.01.057.
[29] Britton TB, Liang H, Dunne FPE, Wilkinson AJ. The effect of crystal orientation on the indentation response of commercially pure titanium: experiments and simulations. Proc R Soc A Math Phys Eng Sci 2010;466(2115):695–719. https://doi.org/10.1098/rspa.2009.0455.

[30] Liu Y, et al. Experimentally quantifying critical stresses associated with basal slip and twinning in magnesium using micropillars. Acta Mater 2017;135:411–21. https://doi.org/10.1016/j.actamat.2017.06.008.
[31] Glechner T, et al. Assessment of ductile character in superhard Ta-C-N thin films. Acta Mater 2019;179:17–25. https://doi.org/10.1016/j.actamat.2019.08.015.
[32] Maier-Kiener V, Schuh B, George EP, Clemens H, Hohenwarter A. Nanoindentation testing as a powerful screening tool for assessing phase stability of nanocrystalline high-entropy alloys. Mater Des 2017;115:479–85. https://doi.org/10.1016/j.matdes.2016.11.055.
[33] Leitner A, Maier-Kiener V, Kiener D. Essential refinements of spherical nanoindentation protocols for the reliable determination of mechanical flow curves. Mater Des 2018;146:69–80. https://doi.org/10.1016/j.matdes.2018.03.003.
[34] Burtscher M, Alfreider M, Schmuck K, Clemens H, Mayer S, Kiener D. In situ fracture observations of distinct interface types within a fully lamellar intermetallic TiAl alloy. J Mater Res 2020. https://doi.org/10.1557/jmr.2020.306.
[35] Barnoush A, Vehoff H. Recent developments in the study of hydrogen embrittlement: hydrogen effect on dislocation nucleation. Acta Mater 2010;58(16):5274–85. https://doi.org/10.1016/j.actamat.2010.05.057.
[36] Vehoff H, Rothe W. Gaseous hydrogen embrittlement. In: FeSi- AND Ni-SINGLE CRYSTALS., no. 30. Pergamon Books Ltd; 1986.
[37] Robertson IM. The effect of hydrogen on dislocation dynamics. Eng Fract Mech 2001;68(6):671–92. https://doi.org/10.1016/S0013-7944(01)00011-X.
[38] Birnbaum HK, Sofronis P. Hydrogen-enhanced localized plasticity-a mechanism for hydrogen-related fracture. Mater Sci Eng 1994;176(1–2):191–202. https://doi.org/10.1016/0921-5093(94)90975-X.
[39] Barnoush A, Vehoff H. In situ electrochemical nanoindentation: a technique for local examination of hydrogen embrittlement. Corrosion Sci 2008;50(1):259–67. https://doi.org/10.1016/j.corsci.2007.05.026.
[40] Ebner AS, Brinckmann S, Plesiutschnig E, Clemens H, Pippan R, Maier-Kiener V. A modified electrochemical nanoindentation setup for probing hydrogen-material interaction demonstrated on a nickel-based alloy. JOM (J Occup Med) 2020;72(5):2020–9. https://doi.org/10.1007/s11837-020-04104-9.
[41] Barnoush A, Vehoff H. Hydrogen embrittlement of aluminum in aqueous environments examined by in situ electrochemical nanoindentation. Scripta Mater 2008;58(9):747–50. https://doi.org/10.1016/j.scriptamat.2007.12.019.
[42] Wang D, Lu X, Deng Y, Guo X, Barnoush A. Effect of hydrogen on nanomechanical properties in Fe-22Mn-0.6C TWIP steel revealed by in-situ electrochemical nanoindentation. Acta Mater 2019;166:618–29. https://doi.org/10.1016/j.actamat.2018.12.055.
[43] Barnoush A, Bies C, Vehoff H. In situ electrochemical nanoindentation of FeAl (100) single crystal: hydrogen effect on dislocation nucleation. J Mater Res 2009;24(3):1105–13. https://doi.org/10.1557/jmr.2009.0084.
[44] Barnoush A, Vehoff H. Electrochemical nanoindentation: a new approach to probe hydrogen/deformation interaction. Scripta Mater 2006;55(2):195–8. https://doi.org/10.1016/j.scriptamat.2006.03.041.
[45] Ebner AS, Plesiutschnig E, Clemens H, Pippan R, Maier-Kiener V. Rate-depending plastic deformation behaviour in a nickel-base alloy under hydrogen influence. Int J Hydrogen Energy 2021;46(76):38132–43. https://doi.org/10.1016/j.ijhydene.2021.09.030.
[46] Duarte MJ, Fang X, Rao J, Krieger W, Brinckmann S, Dehm G. In situ nanoindentation during electrochemical hydrogen charging: a comparison between front-side and a novel back-side charging approach. J Mater Sci 2021. https://doi.org/10.1007/s10853-020-05749-2.
[47] Kim J, Tasan CC. Microstructural and micro-mechanical characterization during hydrogen charging: an in situ scanning electron microscopy study. Int J Hydrogen Energy 2019;44(12):6333–43. https://doi.org/10.1016/j.ijhydene.2018.10.128.
[48] Schober T, Dieker C. Observation of local hydrogen on nickel surfaces. Metall Trans A 1983;14(11):2440–2. https://doi.org/10.1007/BF02663321.
[49] Koyama M, Yamasaki D, Nagashima T, Tasan CC, Tsuzaki K. In situ observations of silver-decoration evolution under hydrogen permeation: effects of grain boundary misorientation on hydrogen flux in pure iron. Scripta Mater 2017;129:48–51. https://doi.org/10.1016/j.scriptamat.2016.10.027.
[50] Deng Y, Hajilou T, Wan D, Kheradmand N, Barnoush A. In-situ micro-cantilever bending test in environmental scanning electron microscope: real time observation of hydrogen enhanced cracking. Scripta Mater 2017;127:19–23. https://doi.org/10.1016/j.scriptamat.2016.08.026.
[51] Deng Y, Barnoush A. Hydrogen embrittlement revealed via novel in situ fracture experiments using notched micro-cantilever specimens. Acta Mater 2018;142:236–47. https://doi.org/10.1016/j.actamat.2017.09.057.
[52] Hajilou T, Deng Y, Rogne BR, Kheradmand N, Barnoush A. In situ electrochemical microcantilever bending test: a new insight into hydrogen enhanced cracking. Scripta Mater 2017;132:17–21. https://doi.org/10.1016/j.scriptamat.2017.01.019.
[53] Wan D, Deng Y, Barnoush A. Hydrogen embrittlement effect observed by in-situ hydrogen plasma charging on a ferritic alloy. Scripta Mater 2018;151(April):24–7. https://doi.org/10.1016/j.scriptamat.2018.03.038.
[54] Wan D, Deng Y, Meling JIH, Alvaro A, Barnoush A. Hydrogen-enhanced fatigue crack growth in a single-edge notched tensile specimen under in-situ hydrogen charging inside an environmental scanning electron microscope. Acta Mater 2019;170:87–99. https://doi.org/10.1016/j.actamat.2019.03.032.
[55] Massone A, et al. An SEM compatible plasma cell for in situ studies of hydrogen-material interaction. Rev Sci Instrum 2020;91(4). https://doi.org/10.1063/1.5142043.
[56] Depover T, Hajilou T, Wan D, Wang D, Barnoush A, Verbeken K. Assessment of the potential of hydrogen plasma charging as compared to conventional electrochemical hydrogen charging on dual phase steel. Mater Sci Eng 2019;754(March):613–21. https://doi.org/10.1016/j.msea.2019.03.097.
[57] Lasia A, Grégoire D. General model of electrochemical hydrogen absorption into metals. J Electrochem Soc 1995;142(10):3393–9. https://doi.org/10.1149/1.2050267.
[58] Shu W, Okuno K, Hayashi Y. Ion-driven permeation of deuterium in metals. Jaeri-M 1993;43.
[59] Mutzke A, et al. SDTrimSP. Garching: Max-Planck-Institut für Plasmaphysik; 2019.
[60] Baskes MI. A calculation of the surface recombination rate constant for hydrogen isotopes on metals. J Nucl Mater 1980;92(2–3):318–24. https://doi.org/10.1016/0022-3115(80)90117-8.
[61] Massone A, et al. Addressing H-material interaction in fast diffusion materials—a feasibility study on a complex phase

steel. Materials Oct 2020;13(20):4677. https://doi.org/10.3390/ma13204677.
[62] Lee JY, Lee SM. Hydrogen trapping phenomena in metals with B.C.C. and F.C.C. crystals structures by the desorption thermal analysis technique. Surf Coating Technol 1986;28(3–4):301–14. https://doi.org/10.1016/0257-8972(86)90087-3.
[63] Zhou H, Hirooka Y, Ashikawa N, Muroga T, Sagara A. Gas- and plasma-driven hydrogen permeation through a reduced activation ferritic steel alloy F82H. J Nucl Mater 2014;455(1–3):470–4. https://doi.org/10.1016/j.jnucmat.2014.07.061.
[64] Doyle BL, Brice DK. Steady state hydrogen transport in solids. Radiat Eff 1985;89(1–2):21–48. https://doi.org/10.1080/00337578508220694.
[65] Asadipoor M, Kadkhodapour J, Pourkamali Anaraki A, Sharifi SMH, Darabi AC, Barnoush A. Experimental and numerical investigation of hydrogen embrittlement effect on microdamage evolution of advanced high-strength dual-phase steel. Met Mater Int 2020. https://doi.org/10.1007/s12540-020-00681-1. 0123456789.
[66] Wang M, Akiyama E, Tsuzaki K. Determination of the critical hydrogen concentration for delayed fracture of high strength steel by constant load test and numerical calculation. Corrosion Sci 2006;48(8):2189–202. https://doi.org/10.1016/j.corsci.2005.07.010.
[67] Klapper HS, Klöwer J, Gosheva O. Hydrogen embrittlement: the game changing factor in the applicability of nickel alloys in oilfield technology. Philos Trans R Soc A Math Phys Eng Sci 2017;375(2098). https://doi.org/10.1098/rsta.2016.0415.
[68] Galliano F, Andrieu E, Blanc C, Cloue JM, Connetable D, Odemer G. Effect of trapping and temperature on the hydrogen embrittlement susceptibility of alloy 718. Mater Sci Eng 2014;611:370–82. https://doi.org/10.1016/j.msea.2014.06.015.
[69] Liu L, Zhai C, Lu C, Ding W, Hirose A, Kobayashi KF. Study of the effect of δ phase on hydrogen embrittlement of Inconel 718 by notch tensile tests. Corrosion Sci 2005;47(2):355–67. https://doi.org/10.1016/j.corsci.2004.06.008.
[70] Tarzimoghadam Z, Ponge D, Klöwer J, Raabe D. Hydrogen-assisted failure in Ni-based superalloy 718 studied under in situ hydrogen charging: the role of localized deformation in crack propagation. Acta Mater 2017;128:365–74. https://doi.org/10.1016/j.actamat.2017.02.059.
[71] Demetriou V, Robson JD, Preuss M, Morana R. Study of the effect of hydrogen charging on the tensile properties and microstructure of four variant heat treatments of nickel alloy 718. Int J Hydrogen Energy 2017;42(37):23856–70. https://doi.org/10.1016/j.ijhydene.2017.02.149.
[72] Lu X, Ma Y, Wang D. On the hydrogen embrittlement behavior of nickel-based alloys: alloys 718 and 725. Mater Sci Eng 2020;792(June). https://doi.org/10.1016/j.msea.2020.139785.
[73] Lu X, Wang D, Wan D, Zhang ZB, Kheradmand N, Barnoush A. Effect of electrochemical charging on the hydrogen embrittlement susceptibility of alloy 718. Acta Mater 2019;179(7491):36–48. https://doi.org/10.1016/j.actamat.2019.08.020.
[74] Zhang Z, Obasi G, Morana R, Preuss M. In-situ observation of hydrogen induced crack initiation in a nickel-based superalloy. Scripta Mater 2017;140:40–4. https://doi.org/10.1016/j.scriptamat.2017.07.006.
[75] Yamada H. Fusion energy. In: Chen WY, Seiner J, Suzuki T, Lackner M, editors. Handbook of climate change mitigation. New York: Springer US; 2012.
[76] Jacob W, Linsmeier C, Rubel M. 13th international workshop on plasma-facing materials and components for fusion applications/1st international conference on fusion energy materials science. Phys Scr T 2011;T145. https://doi.org/10.1088/0031-8949/2011/T145/011001.
[77] Duffy DM. Modeling plasma facing materials for fusion power. Mater Today 2009;12(11):38–44. https://doi.org/10.1016/S1369-7021(09)70297-4.
[78] Roth J, Schmid K. Hydrogen in tungsten as plasma-facing material. Phys Scr T 2011;T145. https://doi.org/10.1088/0031-8949/2011/T145/014031.
[79] Manhard A, Schmid K, Balden M, Jacob W. Influence of the microstructure on the deuterium retention in tungsten. J Nucl Mater 2011;415(1 SUPPL):S632–5. https://doi.org/10.1016/j.jnucmat.2010.10.045.
[80] Gao L, et al. Deuterium supersaturation in low-energy plasma-loaded tungsten surfaces. Nucl Fusion 2017;57(1):16026. https://doi.org/10.1088/0029-5515/57/1/016026.
[81] Zayachuk Y, Manhard A, 'T Hoen MHJ, Jacob W, Zeijlmans Van Emmichoven PA, Van Oost G. Depth profiling of the modification induced by high-flux deuterium plasma in tungsten and tungsten-tantalum alloys. Nucl Fusion 2014;54(12). https://doi.org/10.1088/0029-5515/54/12/123013.
[82] Yoon HK, Lee SH, Kang SJL, Yoon DN. Effect of vacuum-treatment on mechanical properties of W-Ni-Fe heavy alloy. J Mater Sci 1983;18(5):1374–80. https://doi.org/10.1007/BF01111957.
[83] Li M, Ruprecht D, Kracker G, Höschen T, Neu R. Impact of heat treatment on tensile properties of 97W–2Ni–1Fe heavy alloy. J Nucl Mater 2018;512:1–7. https://doi.org/10.1016/j.jnucmat.2018.09.055.
[84] Bellosta von Colbe J, et al. Application of hydrides in hydrogen storage and compression: achievements, outlook and perspectives. Int J Hydrogen Energy 2019;44(15):7780–808. https://doi.org/10.1016/j.ijhydene.2019.01.104.
[85] Zhang L, Wen M, Imade M, Fukuyama S, Yokogawa K. Effect of nickel equivalent on hydrogen gas embrittlement of austenitic stainless steels based on type 316 at low temperatures. Acta Mater 2008;56(14):3414–21. https://doi.org/10.1016/j.actamat.2008.03.022.
[86] Murakami Y, Kanezaki T, Mine Y, Matsuoka S. Hydrogen embrittlement mechanism in fatigue of austenitic stainless steels. Metall Mater Trans A Phys Metall Mater Sci 2008;39 A(6):1327–39. https://doi.org/10.1007/s11661-008-9506-5.
[87] Talonen J, Hänninen H. Formation of shear bands and strain-induced martensite during plastic deformation of metastable austenitic stainless steels. Acta Mater 2007;55(18):6108–18. https://doi.org/10.1016/j.actamat.2007.07.015.
[88] Michler T, Yukhimchuk AA, Naumann J. Hydrogen environment embrittlement testing at low temperatures and high pressures. Corrosion Sci 2008;50(12):3519–26. https://doi.org/10.1016/j.corsci.2008.09.025.
[89] Michler T, San Marchi C, Naumann J, Weber S, Martin M. Hydrogen environment embrittlement of stable austenitic steels. Int J Hydrogen Energy 2012;37(21):16231–46. https://doi.org/10.1016/j.ijhydene.2012.08.071.
[90] Han G, He S, Fukuyama S, Yokogawa K. Effect of nickel equivalent on hydrogen environment embrittlement of austenitc stainless steels at low temperatures. Acta Mater 1998;46(13). 4599–4570.
[91] Koyama M, et al. Hydrogen desorption and cracking associated with martensitic transformation in Fe-Cr-Ni-Based austenitic steels with different carbon contents. Int J Hydrogen Energy 2017;42(42):26423–35. https://doi.org/10.1016/j.ijhydene.2017.08.209.
[92] Vennet RM, Ansell GS. The effect of high-pressure hydrogen upon tensile properties and fracture behavior of 304L stainless steel. Trans ASM 1967;60:242–51.

[93] Benson RB, Dann RK, Roberts LW. Hydrogen embrittlement of stainless steel. Trans AIME 1968;242:2199–205.
[94] Jr RCB, Fultz B. M etallic hydrides I : and other gas- phase Applications. Mater Res Soc 2002:688–93. September.
[95] Libowitz GG. Metallic hydrides; fundamental properties and applications. J Phys Chem Solid 1994;55(12):1461–70. https://doi.org/10.1016/0022-3697(94)90571-1.
[96] Joubert J, Latroche M. M etallic hydrides II : electrochemical storage. 2020. September 2002.
[97] Weast RC, Astle MJ, Beyer WH. CRC handbook of chemistry and physics. 64th ed. Boca Raton, Florida: CRC Press; 1983.
[98] Trudeau ML. Advanced materials for energy storage. MRS Bull Nov. 1999;24(11):23–6. https://doi.org/10.1557/S0883769400053410.
[99] Yu H, Hebling C, Revathi S. Fuel cells: microsystems. Ref Modul Mater Sci Mater En. 2016:1–15. https://doi.org/10.1016/b978-0-12-803581-8.01727-6. September 2015.
[100] Olabi AG, Wilberforce T, Abdelkareem MA. Fuel cell application in the automotive industry and future perspective. Energy 2021;214:118955. https://doi.org/10.1016/j.energy.2020.118955.
[101] Louthan MR. Hydrogen embrittlement of metals: a primer for the failure analyst. J Fail Anal Prev 2008;8(3 SPEC):289–307. https://doi.org/10.1007/s11668-008-9133-x.
[102] Drexler A, et al. On the local evaluation of the hydrogen susceptibility of cold-formed and heat treated advanced high strength steel (AHSS) sheets. Mater Sci Eng 2021;800(June 2020):140276. https://doi.org/10.1016/j.msea.2020.140276.
[103] Loidl M, Kolk O, Veith S, Göbel T. Characterization of hydrogen embrittlement in automotive advanced high strength steels. Mater Werkst 2011;42(12):1105–10. https://doi.org/10.1002/mawe.201100917.
[104] Venezuela J, Liu Q, Zhang M, Zhou Q, Atrens A. A review of hydrogen embrittlement of martensitic advanced high-strength steels. Corrosion Rev 2016;34(3):153–86. https://doi.org/10.1515/corrrev-2016-0006.
[105] Figueroa D, Robinson MJ. The effects of sacrificial coatings on hydrogen embrittlement and re-embrittlement of ultra high strength steels. Corrosion Sci 2008;50(4):1066–79. https://doi.org/10.1016/j.corsci.2007.11.023.
[106] Krylova I. Painting by electrodeposition on the eve of the 21st century. Prog Org Coating 2001;42(3–4):119–31. https://doi.org/10.1016/S0300-9440(01)00146-1.
[107] Lovicu G, et al. Hydrogen embrittlement of automotive advanced high-strength steels. Metall Mater Trans A Phys Metall Mater Sci 2012;43(11):4075–87. https://doi.org/10.1007/s11661-012-1280-8.
[108] Hardie D, Charles EA, Lopez AH. Hydrogen embrittlement of high strength pipeline steels. Corrosion Sci 2006;48(12):4378–85. https://doi.org/10.1016/j.corsci.2006.02.011.
[109] Liu Y, Wang M, Liu G. Effect of hydrogen on ductility of high strength 3Ni-Cr-Mo-V steels. Mater Sci Eng 2014;594:40–7. https://doi.org/10.1016/j.msea.2013.11.058.
[110] Li X, Wang Y, Zhang P, Li B, Song X, Chen J. Effect of pre-strain on hydrogen embrittlement of high strength steels. Mater Sci Eng 2014;616:116–22. https://doi.org/10.1016/j.msea.2014.07.085.
[111] Depover T, Pérez Escobar D, Wallaert E, Zermout Z, Verbeken K. Effect of hydrogen charging on the mechanical properties of advanced high strength steels. Int J Hydrogen Energy 2014;39(9):4647–56. https://doi.org/10.1016/j.ijhydene.2013.12.190.
[112] Hilditch TB, Lee SB, Speer JG, Matlock DK. Response to hydrogen charging in high strength automotive sheet steel products. SAE Tech Pap; 2003. https://doi.org/10.4271/2003-01-0525. 724.
[113] Rehrl J, Mraczek K, Pichler A, Werner E. Mechanical properties and fracture behavior of hydrogen charged AHSS/UHSS grades at high- and low strain rate tests. Mater Sci Eng 2014;590:360–7. https://doi.org/10.1016/j.msea.2013.10.044.
[114] Duprez L, Verbeken K, Verhaege M. Effect of hydrogen on the mechanical properties of multiphase high-strength steels. In: International hydrogen conference: Effects of hydrogen on materials; 2008.